Retarded radiation from colliding black holes in the close limit

Sascha Husa,[1,2] Yosef Zlochower,[2] Roberto Gómez,[2,3] and Jeffrey Winicour[1,2]
[1]*Albert Einstein Institute, Max Planck Gesellschaft, Haus 1, Am Mühlenberg, Golm, Germany*
[2]*Department of Physics and Astronomy, University of Pittsburgh, Pittsburgh, Pennsylvania 15260*
[3]*Pittsburgh Supercomputing Center, 4400 Fifth Avenue, Pittsburgh, Pennsylvania 15213*
(Received 30 August 2001; published 8 April 2002)

We use null hypersurface techniques in a new approach to calculate the retarded waveform from a binary black hole merger in the close approximation. The process of removing ingoing radiation from the system leads to two notable features in the shape of the close approximation waveform for a head-on collision of black holes: (i) an initial quasinormal ringup and (ii) weak sensitivity to the parameter controlling the collision velocity. Feature (ii) is unexpected and has the potential importance of enabling the design of an efficient template for extracting the gravitational wave signal from the noise.

DOI: 10.1103/PhysRevD.65.084034 PACS number(s): 04.20.Ex, 04.25.Dm, 04.25.Nx, 04.70.Bw

I. INTRODUCTION

We use a characteristic evolution algorithm to compute the retarded radiation produced by the vacuum collision of two black holes in the close approximation where the collision occurs in the distant past. The retarded wave corresponds to the perturbation of a Schwarzschild spacetime in which no ingoing radiation enters the system. In previous work [1] we applied characteristic evolution to determine the close approximation retarded waveform from a white hole fission. Here we find that the retarded waveform from a black hole merger has distinct features which do not appear in the fission waveform: (i) an initial quasinormal ringup and (ii) weak sensitivity to the parameter controlling the collision time scale. Feature (i) arises at early times as a mathematical artifact of eliminating ingoing radiation in a vacuum black hole evolution. This feature, which we expect would also arise in an analogous Cauchy treatment of the problem, is not of physical significance for black holes which are formed in the past from collapsing matter in a conventional astrophysical scenario. On the other hand, feature (ii) arises at the intermediate time just prior to the ringdown of the final black hole. Removal of incoming waves that would affect the intermediate time waveform is essential in order to ensure that the outgoing radiation is due to the black holes rather than the initial radiation content of the gravitational field. Feature (ii) has potential observational importance for the design of an efficient template for extracting gravitational waves from detector noise.

In a conventional astrophysical scenario, colliding black holes arise when each star in a binary undergoes gravitational collapse and the two resulting black holes inspiral and merge. Unfortunately, the full simulation of such a system is presently far beyond the state-of-the-art in numerical relativity. As a consequence, computational studies of black hole collisions have so far been restricted to the vacuum case. Furthermore, numerical instabilities in dealing with the strong fields of black holes have limited Cauchy evolution to short times. (See Refs. [2,3] for recent results.) Long term simulations have only been achieved by introducing a perturbative treatment but even in this case there have been no evolutions backward in time to determine the radiation content of the Cauchy data. The close approximation [4], based on the perturbation of a stationary single black hole spacetime, has been extremely useful for understanding the binary black hole problem by means of Cauchy evolution [5–14]. Even in a Schwarzschild background, the absence of any analytic linearized solutions makes a computational approach necessary. However, the perturbative equations can be evolved with high accuracy and provide the closest thing to an exact solution for calibrating the accuracy of a fully nonlinear code, as has become practice [15–17].

Perturbation approximations play a similar role in calibrating the accuracy of characteristic evolution codes and testing their ability to give reliable physical information [18]. Our previous paper [1], which uses characteristic evolution to compute the close approximation retarded waveform for a white hole fission, is the starting point for the present work. Under time reversal, the retarded solution for a white hole fission is equivalent to an advanced solution for a black hole merger. In the advanced solution, ingoing radiation is absorbed by the black holes but no outgoing radiation is emitted. This advanced solution [1] provides stage I of a new two stage approach to the binary black hole problem [19–21]. In stage II, treated here, we present the physically appropriate retarded waveform for a black hole collision in which there is no ingoing radiation from past null infinity $\mathcal{I}^-$ in the background Schwarzschild spacetime.

These perturbative results furnish a reference point for the physical understanding of a fully nonlinear version of the same approach [19–21] which is being pursued using existing characteristic evolution codes [18,22]. They also complement the physical picture obtained in this approximation by Cauchy evolution.

The advanced solution for a black hole merger is simpler to compute in a characteristic approach because of the relative location of the two null hypersurfaces on which boundary information is known. One of the null hypersurfaces is the black hole event horizon $\mathcal{H}^+$, whose perturbation corresponds to the close approximation of a binary black hole. In the advanced problem, the other null hypersurface (in a conformally compactified description) is future null infinity $\mathcal{I}^+$ where the outgoing radiation vanishes. Since $\mathcal{H}^+$ and $\mathcal{I}^+$ formally intersect at future time infinity I^+, they can be used

to pose a double-null initial value problem [23–26] to evolve backward in time and compute the exterior region of spacetime. (Potential difficulties in dealing with I^+ are avoided by posing the problem on an ingoing null hypersurface $\mathcal{J}^+$ which approximates $\mathcal{I}^+$ and intersects $\mathcal{H}^+$ at a late time when the perturbation has effectively died out.) On the other hand, in the retarded problem, the other null hypersurface is past null infinity $\mathcal{I}^-$ where the ingoing radiation is required to vanish. Because $\mathcal{H}^+$ and $\mathcal{I}^-$ are disjoint, there is no direct way to base a characteristic initial value problem on these two hypersurfaces.

The advanced solution provides the ingoing radiation incident from $\mathcal{I}^-$. In the context of linear perturbation theory, the time translation and reflection symmetries of the background provide a mathematically well defined way to carry out stage II by using this ingoing radiation to generate a ''source free'' *advanced minus retarded* solution. A retarded solution is then produced by superposition with the stage I solution. In this paper, we deal with the subtleties produced in implementing this procedure and compute, for the first time, a perturbative solution with no ingoing radiation.

Time reflection symmetry allows the merger of two black holes to be described as the fission of a white hole. It is convenient here for computational purposes to formulate the binary black hole problem in this time reversed sense as a white hole fission since the characteristic evolution then takes the standard form of being carried out forward in retarded time. From a time reversed point of view, the stage I solution is equivalent to the retarded solution for a white hole fission, with the physically appropriate boundary conditions that radiation is emitted but that there is no ingoing radiation from $\mathcal{I}^-$; and, under time reversal, the stage II solution is equivalent to the advanced solution for a white hole fission, with the boundary condition that radiation from $\mathcal{I}^-$ is absorbed but no outgoing radiation is emitted. Although time reflection maps a black hole merger into a white hole fission, imposition of a retarded wave boundary condition makes the resulting waveform markedly different in physical character. This is because the radiation from a white hole merger can travel directly to $\mathcal{I}^+$ whereas any black hole process only produces radiation at $\mathcal{I}^+$ indirectly from the prior events leading to black hole formation.

In Sec. II, we review the background material upon which this work is based [1]. We use a characteristic reformulation of the Teukolsky equations [27] governing the perturbative Weyl tensor. Previous work dealt with a characteristic evolution algorithm for solving the Teukolsky equation for the ingoing null component of the Weyl tensor [1]. In order to carry out stage II, we extend this work to an evolution algorithm for evolving the outgoing null component. Characteristic data obtained for the nonlinear description of a binary black hole spacetime is used to induce close approximation data for the perturbative solution considered here.

In Sec. III, we provide the technical details of our global strategy for producing the retarded waveform from a black hole process. In Sec. IV, we describe the numerical implementation and testing of the evolution algorithm. Because of difficult computational problems of a global nature, we develop two independent evolution algorithms and carry out extensive testing in order to demonstrate that the final waveform is free of numerical artifacts.

In Sec. V, we present the properties of the retarded waveform from a head-on black hole collision in the close approximation. It has been suggested that the black hole merger waveform might have a distinct signature that is roughly independent of the details of the initial conditions. Our results do confirm the generally accepted view that the waveform has a quasinormal ringdown stage characteristic of the final black hole mass (which is here the background mass). However, we find that the features of the main waveform are sensitive to the presence of ingoing radiation fields of the type that would be present, for instance, in the evolution of time reflection symmetric Cauchy data.

Notation and Conventions: We use a metric of signature $(-+++)$ and a null tetrad with normalization $l^a n_a = -m^a \bar{m}_a = -1$, so that $g_{ab} = 2(m_{(a}\bar{m}_{b)} - l_{(a}n_{b)})$. We introduce standard angular coordinates $x^A = (\theta, \phi)$ to represent the unit sphere metric q_{AB} and set $q^{AB} = q^{(A}\bar{q}^{B)}$, where $q^{AB}q_{BC} = \delta^A_C$, with $q^A = (1, i/\sin\theta)$. We use q^A to define the $\eth$ operator with the convention $\eth f = q^A \partial_A f$, for a spin-weight 0 function f. Complex conjugation is denoted with a ''bar,'' e.g. $\Re(f) = (f + \bar{f})/2$. These conventions lead to a different form of the perturbation equations from that originally given by Teukolsky.

II. BACKGROUND FORMALISM

Various coordinates were used in Ref. [1] to describe curvature perturbations of a Schwarzschild background. The simplest global choice are Israel coordinates [28] in which the Schwarzschild metric takes the form

$$ds^2 = -W du^2 - 2du d\lambda + r^2 q_{AB} dx^A dx^B, \tag{2.1}$$

where u is an affine parameter along the ingoing null hypersurface $r = 2M$ that forms the white hole horizon, λ is an affine parameter along the outgoing null geodesics in the direction of increasing $r = 2M - \lambda u/(4M)$ and

$$W = \frac{2\lambda^2}{\lambda u - 8M^2}. \tag{2.2}$$

[Affine freedom has been used to set $\lambda = 0$ on the white hole horizon, to set $u = 0$ at the $r = 2M$ bifurcation sphere between the black hole and white hole horizons and to set $g^{ab}(\partial_a u)\partial_b \lambda = -1$.] Israel coordinates cover the entire Kruskal manifold with nonsingular and simple analytic behavior. The exterior quadrant is given by $u < 0$, $\lambda > 0$.

Other coordinates more suitable for certain numerical purposes are outgoing Eddington-Finkelstein coordinates $(\tilde{u}, r)$, in which the Schwarzschild metric is

$$ds^2 = -\left(1 - \frac{2M}{r}\right) d\tilde{u}^2 - 2 d\tilde{u} dr + r^2 d\Omega^2. \tag{2.3}$$

Here $u = -M e^{-\tilde{u}/4M}$ and $\tilde{u}$ is a Bondi retarded time coordinate related to the standard Schwarzschild time coordinate t

by $\tilde{u}=t-r^*$, with $r^*=r+2M\log(r/2M-1)$. These outgoing Eddington-Finkelstein coordinates patch the lower half of the Kruskal manifold composed of the exterior quadrant and the quadrant above the initial singularity, with $\tilde{u}\to\infty$ at the black hole horizon.

Israel coordinates induce the nonsingular complex null tetrad

$$l^a=-\nabla^a u=\left(\frac{\partial}{\partial\lambda}\right)^a=[0,1,0,0],$$

$$n^a=\left(\frac{\partial}{\partial u}\right)^a-\frac{W}{2}\left(\frac{\partial}{\partial\lambda}\right)^a=\left[1,\frac{\lambda^2}{4Mr},0,0\right],$$

$$m^a=\frac{1}{\sqrt{2}r}q^a,$$

$$\overline{m}^a=\frac{1}{\sqrt{2}r}\overline{q}^a, \tag{2.4}$$

where

$$q^a=\left(\frac{\partial}{\partial\theta}\right)^a+\frac{i}{\sin\theta}\left(\frac{\partial}{\partial\phi}\right)^a=[0,0,q^A]. \tag{2.5}$$

The Teukolsky equations [27] for the vacuum perturbation of the outgoing null component of Weyl curvature, $\psi_0=C_{abcd}l^a m^b l^c m^d$ (in Newman-Penrose notation [29]) and the ingoing null component $\psi_4=C_{abcd}n^a\overline{m}^b n^c\overline{m}^d$ are

$$\left(L_0+\frac{L^2}{2r^2}\right)\psi_0=0 \quad \text{and} \quad \left(L_4+\frac{L^2}{2r^2}\right)\psi_4=0, \tag{2.6}$$

where

$$L_0=\frac{1}{4Mr}\lambda^2\partial_\lambda^2+\partial_u\partial_\lambda-\frac{5}{4Mr}u\partial_u$$
$$-\frac{1}{2Mr^2}\lambda(3M-4r)\partial_\lambda+\frac{5}{2rM},$$

$$L_4=\frac{1}{4Mr}\lambda^2\partial_\lambda^2+\partial_u\partial_\lambda-\frac{1}{4Mr}u\partial_u$$
$$-\frac{7}{2r^2}\lambda\partial_\lambda-\frac{r^2-16M^2+4Mr}{2Mr^3} \tag{2.7}$$

and $L^2=-\bar{\eth}\eth$ is the angular momentum squared operator.

The Weyl components ψ_0 and ψ_4 have spin-weight $s=2$ and $s=-2$, respectively. It is useful to convert Eqs. (2.6), (2.7) into spin-weight-zero equations by setting $\psi_0=\eth^2\Phi_0$ and $\psi_4=\bar{\eth}^2\Phi_4$. Furthermore, the computation of asymptotic behavior is enhanced by working with the fields $F_0=r^5\Phi_0$ and $F_4=r\Phi_4$, which generically have finite non-vanishing limits at $\mathcal{I}^+$ for asymptotically flat perturbations.

Although the Weyl scalars formed from the (l^a,n^a) null vectors are non-singular in the full Kruskal manifold, they are not well adapted for numerical accuracy. In order to compute radiation at late times near $\mathcal{I}^+$ it is advantageous to consider a boosted tetrad $(\tilde{l}^a,\tilde{n}^a,m^a,\overline{m}^a)$, with $\tilde{l}^a=-\nabla^a\tilde{u}$ and satisfying $\tilde{l}^a\tilde{n}_a=-1$, which is adapted to Bondi time $\tilde{u}$ at $\mathcal{I}^+$ rather than the affine horizon time u. We denote the corresponding Weyl components by $\tilde{\psi}_0=C_{abcd}\tilde{l}^a m^b\tilde{l}^c m^d$ and $\tilde{\psi}_4=C_{abcd}\tilde{n}^a\overline{m}^b\tilde{n}^c\overline{m}^d$. In particular, the late time behavior of the radiation waveform can be more accurately computed by an evolution algorithm for the Weyl component $\tilde{\psi}_4$.

Setting $\tilde{\psi}_0=\eth^2\tilde{\Phi}_0$ and $\tilde{\psi}_4=\bar{\eth}^2\tilde{\Phi}_4$, the Teukolsky equations for the fields $\tilde{F}_0=r^5\tilde{\Phi}_0$ and $\tilde{F}_4=r\tilde{\Phi}_4$ reduce to the spin-weight zero forms

$$(D^2+S_0)\tilde{F}_0=0, \tag{2.8}$$

$$(D^2+S_4)\tilde{F}_4=0, \tag{2.9}$$

where

$$S_0=\frac{16M(r-3M)}{ur^2}\partial_\lambda-\frac{30M}{r^3}+\frac{(6+\bar{\eth}\eth)}{r^2}$$
$$=-\frac{4(r-3M)}{r^2}\partial_r-\frac{30M}{r^3}+\frac{(6+\bar{\eth}\eth)}{r^2} \tag{2.10}$$

and

$$S_4=-\frac{16M(r-3M)}{ur^2}\partial_\lambda-\frac{6M}{r^3}+\frac{(2+\bar{\eth}\eth)}{r^2}$$
$$=\frac{4(r-3M)}{r^2}\partial_r-\frac{6M}{r^3}+\frac{(2+\bar{\eth}\eth)}{r^2}, \tag{2.11}$$

and

$$D^2=-\frac{2\lambda(16M^2-u\lambda)}{(8M^2-u\lambda)^2}\partial_\lambda-2\partial_u\partial_\lambda$$
$$-\frac{2\lambda^2}{8M^2-u\lambda}\partial_\lambda^2, \tag{2.12}$$

is the Laplacian defined by the metric $d\overline{s^2}=-(1-2M/r)d\tilde{u}^2-2d\tilde{u}dr$ induced by the background on the 2-dimensional $(\tilde{u},r)$ subspace. Equations (2.10) and (2.11) asymptote to one-dimensional wave equations for solutions whose radial derivative falls off uniformly as $O(1/r^2)$. The limit of $\tilde{F}_4$ determines the outgoing gravitational radiation waveform while the limit of $\tilde{F}_0$ is related to the retarded

quadrupole moment of the system. More precisely, $\lim r\tilde{\psi}_4 = \partial_{\tilde{u}}\overline{N}$, where N is the standard definition of the Bondi news function.

In these variables, the deviation of Eqs. (2.8) and (2.9) from a 1-dimensional wave equation is independent of time at a fixed r. Because $\tilde{F}_4=(u/4M)^2F_4$, where F_4 is regular throughout the Kruskal manifold (since it is constructed with a regular basis), it follows that $\tilde{F}_4\to 0$ as the black hole horizon is approached. This facilitates an accurate long term evolution of the waveform using Eq. (2.9).

In contrast, $\tilde{F}_0=(4M/u)^2F_0$, so that $\tilde{F}_0$ is singular on the black hole horizon, and thus a poor choice of variable for long term evolution. The opposite signs of the coefficients of ∂_r in S_0 and S_4 are responsible for this behavior, as can be seen by ignoring the remaining potential terms and freezing the coefficient of ∂_r at $r=2M$, so that Eqs. (2.8) and (2.9) reduce to

$$\left(2\partial_{\tilde{u}}-\partial_r-\frac{1}{M}\right)\partial_r\tilde{F}_0=0, \tag{2.13}$$

$$\left(2\partial_{\tilde{u}}-\partial_r+\frac{1}{M}\right)\partial_r\tilde{F}_4=0, \tag{2.14}$$

in terms of retarded Bondi coordinates. In this approximation, both of these equations admit purely outgoing waves $\tilde{F}(\tilde{u})$. However, an ingoing $\tilde{F}_0$ wave has the exponentially singular behavior

$$\tilde{F}_0=f(\tilde{u}+2r)e^{(\tilde{u}-\tilde{u}_0)/2M} \tag{2.15}$$

as an initial pulse $f(\tilde{u}_0+2r)$ approaches the black hole horizon as $\tilde{u}\to\infty$. An ingoing $\tilde{F}_4$ wave behaves in an opposite fashion and decays exponentially on approach to the black hole.

The different forms of Eqs. (2.8) and (2.9) make it clear that the Weyl component ψ_0 in the outgoing null direction l^a and the Weyl component ψ_4 in the ingoing null direction n^a are not related in a way which makes manifest the Schwarzschild time reflection symmetry $\mathcal{T}$, defined by $\mathcal{T}(t,r,\theta,\phi)=(-t,r,\theta,\phi)$ in Schwarzschild coordinates or by $\mathcal{T}(\tilde{u},r,\theta,\phi)=(-\tilde{v},r,\theta,\phi)$ in terms of Bondi retarded and advanced times $\tilde{u}=t-r^*$ and $\tilde{v}=t+r^*$. The time reflection symmetry could be incorporated explicitly into the pair of Teukolsky equations by introducing null tetrad vectors $L^a=\alpha l^a$ and $N^a=(1/\alpha)n^a$ satisfying $\mathcal{T}L^a=-N^a$. However, the explicit form of the required boost,

$$\alpha=-\frac{2M}{u}\sqrt{\frac{2(r-2M)}{r}}=-\frac{2M}{u}\sqrt{\frac{-2\lambda u}{8M^2-\lambda u}}, \tag{2.16}$$

makes it clear that such a time symmetric formulation would introduce singular behavior at both the black and white hole horizons.

This time symmetric tetrad is useful for formulating the time reflection properties of solutions of the Teukolsky equations using other tetrads. Let $\Psi_4=C_{abcd}N^a\overline{m}^bN^c\overline{m}^d=\Psi(\tilde{u},r,\theta,\phi)$ be a perturbative solution for Ψ_4. Then the time reflection symmetry implies that $\Psi_0=C_{abcd}L^am^bL^cm^d=\overline{\Psi}(-\tilde{v},r,\theta,\phi)$ is a perturbative solution for Ψ_0. This correspondence maps a retarded solution (no incoming radiation) for Ψ_4 into an advanced solution (no outgoing radiation) for Ψ_0. In terms of the $\tilde{l}^a$ and $\tilde{n}^a$ Weyl components, the solution $\tilde{\psi}_4=\tilde{\psi}(\tilde{u},r,\theta,\phi)$ corresponds under time reflection to the solution

$$\tilde{\psi}_0=\frac{4r^2}{(r-2M)^2}\overline{\psi}(-\tilde{v},r,\theta,\phi). \tag{2.17}$$

A. Close approximation data

Data for the double-null formulation of the characteristic initial value problem are given on a pair of intersecting null hypersurfaces. The data for a fissioning white hole are posed on the ingoing null hypersurface $\mathcal{H}^-$ and an early outgoing null hypersurface $\mathcal{J}^-$, which extends from $\mathcal{H}^-$ to $\mathcal{I}^+$. In Ref. [1], consistent double-null data for ψ_4 for a fissioning white hole were obtained from the metric data for the nonlinear version of the problem in terms of a spin-weight-2 field J describing the inner conformal geometries of $\mathcal{H}^-$ and $\mathcal{J}^-$ [20].

The underlying field J for a white hole fission is provided by a conformal model based upon an ingoing null hypersurface $\mathcal{N}$ emanating from a prolate spheroid embedded in a flat space [30,31]. Let $(\hat{r},\theta,\phi)$ be standard spherical coordinates for the inertial time slices $\hat{t}=$const of Minkowski space. When the eccentricity of the spheroid vanishes, the Minkowski null hypersurface reduces to the light cone from a sphere $\hat{t}=0$, $\hat{r}=a$. The intrinsic geometry of $\mathcal{N}$ is described by a degenerate rank-2 metric $\hat{r}^2h_{AB}$ where $J=q^Aq^Bh_{AB}$. To linear order in the eccentricity, the conformal model gives

$$J(\hat{t},\theta)=-\frac{a\sin^2\theta}{\hat{t}-a}. \tag{2.18}$$

This conformal geometry of $\mathcal{N}$ models the conformal geometry of the white hole horizon $\mathcal{H}^-$ in the close limit where the fission occurs in the infinite future. The area coordinate r of the geometry of $\mathcal{H}^-$ differs from the corresponding $\hat{r}$ of the geometry of $\mathcal{N}$ in order to yield an asymptotically constant surface area for the initial white hole in the infinite past. For vanishing eccentricity, this produces a Schwarzschild horizon and a small eccentricity generates the close approximation.

The Raychaudhuri equation, which governs the expansion of a null hypersurface, forces a difference in the affine parameters on $\mathcal{N}$ and $\mathcal{H}^-$. With a suitable choice of affine scale, the relation between $\hat{t}$ and the affine parameter u on the white hole horizon is

$$\frac{d\hat{t}}{du}=\Lambda(\hat{\tau})=\frac{\hat{\tau}^2(\hat{\tau}-1)^2}{(3-5\hat{\tau}+\hat{\tau}^2)^2}\left(\frac{(5-\sqrt{13})-2\hat{\tau}}{(5+\sqrt{13})-2\hat{\tau}}\right)^{4/\sqrt{13}}, \tag{2.19}$$

where $\hat{\tau}=\hat{t}-a$. At early times Eq. (2.19) implies $u\sim\hat{t}$ but as the Minkowski null cone pinches off at $\hat{t}=a$ the corresponding affine time on the white hole horizon asymptotes to $u\to\infty$. In terms of the inverted pair-of-pants picture for a white hole fission, the pants legs are mapped to $u=\infty$, so that in the close limit the individual white holes are mapped to future infinity along the white hole horizon in the Kruskal manifold. The details are discussed elsewhere in a treatment of fully nonlinear null data for the general two black hole problem [20,31].

Close limit data for $J(u,\theta)$ on the white hole horizon are determined by integrating Eq. (2.19) and substituting into Eq. (2.18). In order to eliminate nonessential integration constants, we set $u=0$ at the $r=2M$ bifurcation sphere. Then, up to scale, the close data are determined by the single parameter

$$\eta=-\frac{J|_{u=0}}{uJ|_{u=\infty}}=-\frac{1}{\hat{\tau}|_{u=0}}, \tag{2.20}$$

where $\eta>0$ is a scale invariant parameter determining the yield of the white hole fission. (In the time reversed scenario of a black hole collision, η is related to the inelasticity of the collision.) In the linear approximation,

$$\overline{\psi}_4\approx\frac{1}{2}J_{,uu}. \tag{2.21}$$

In this way, the conformal horizon model determines the close limit data for ψ_4 on the horizon $\mathcal{H}^-$. By choosing $\mathcal{J}^-$ to be an early outgoing null hypersurface approximating $\mathcal{I}^-$, we prescribe data $\psi_4=0$ on $\mathcal{J}^-$, which is consistent with the asymptotic falloff $\psi_4=O(u^{-3})$ along $\mathcal{H}^-$ implied by Eq. (2.18). This approximates the condition that there be no ingoing radiation from $\mathcal{I}^-$.

In terms of the spin-weight-zero potential F_4, the close data on $\mathcal{H}^-$ have the normalized form

$$F_4=-(\Lambda\partial_{\hat{\tau}})(\Lambda\partial_{\hat{\tau}})\frac{1}{\hat{\tau}}, \tag{2.22}$$

after factoring out the $l=2$ angular dependence.

The time dependence of the close approximation data is quite mild when expressed as a function of $\hat{\tau}$, as in Eq. (2.22). However, the relationship (2.19) produces a sharp transition region where the behavior of $\hat{\tau}(u)$ changes from the asymptotic form $d\hat{\tau}/du\to1$ as $\hat{\tau}\to-\infty$ to $d\hat{\tau}/du\to0$ as $\hat{\tau}\to0$ [20]. For large values of the parameter η, this produces sharply pulse shaped data [1].

III. COMPUTING RETARDED WAVEFORMS FROM BLACK HOLES

A. Removing the ingoing radiation

In the time reversed scenario being pursued here, our strategy for computing the retarded solution for a black hole collision is based upon the computation of the advanced solution from a white hole fission. Stage I of the approach, i.e. computation of the retarded solution for a white hole fission, has already been carried out [1]. Close approximation data for ψ_4 provided by the conformal horizon model was evolved to determine the stage I solution $\psi_{4,I}$ throughout the exterior region of spacetime. In practice, the evolution computes the corresponding spin-weight-0 potential $\tilde{F}_{4,I}$, whose value on $\mathcal{I}^+$ determines the outgoing radiation field $\tilde{F}_{4,I,OUT}$. In stage I of the white hole problem, there is no ingoing radiation from $\mathcal{I}^-$. In stage II, the strategy for converting the retarded solution to an advanced solution with no outgoing radiation is to superpose a perturbative solution whose outgoing field equals $-\tilde{F}_{4,I,OUT}$.

This procedure for converting from an advanced to a retarded field in a white hole spacetime differs from the standard procedure in a flat spacetime. The retarded solution Φ_{RET} of the flat space wave equation $\Box\Phi=S$ with source S may be converted into the advanced solution Φ_{ADV} by superposing the source free (homogeneous) solution $H=\Phi_{ADV}-\Phi_{RET}$. In the vacuum white hole (or black hole) problem, there is no source in the exterior spacetime. The white hole horizon itself acts as the source of the exterior solution. In this vein, specification of the ''source-free'' solution which transforms a retarded white hole perturbation to an advanced white hole perturbation requires specification of horizon data on $\mathcal{H}^+$ as well as the outgoing data $-\tilde{F}_{4,I,OUT}$ at $\mathcal{I}^+$. These horizon data must not introduce any features which change the physical interpretation of the system as a white hole fission. For example, it is essential not to superpose a black hole merger on the white hole fission, as this would result in the specification of a Cauchy problem with time symmetric data.

We carry out the conversion to an advanced solution by evolving backward in time the double null problem with data $\tilde{F}_4=0$ on the black hole horizon $\mathcal{H}^+$ and data $\tilde{F}_4=-F_{4,I,OUT}$ at $\mathcal{I}^+$. These data leave the black hole horizon unchanged and its evolution determines the analogue of the ''homogeneous solution'' H. The superposition $\tilde{F}_{4,II}=\tilde{F}_{4,I}+H$ then produces the desired advanced solution for a white hole fission with no outgoing radiation. The stage II solution leaves the black hole horizon unchanged but perturbs the white hole, essentially making it ring. In the time reversed black hole scenario, this is a physically desirable effect because the binary black hole data provided by the conformal horizon model has a power law decay in u, which corresponds to a purely exponential decay in $\tilde{u}$ without quasinormal oscillations. *A priori* introduction of ringdown in the final black hole data would be artificial. In stage II, the conversion from an advanced to retarded binary black hole so-

lution automatically introduces this ringdown in a natural way in addition to removing the ingoing radiation.

B. Producing the outgoing waveform

The Weyl components $\tilde{\psi}_0$ and $\tilde{\psi}_4$ form the major part of the geometrical description of a Schwarzschild perturbation. The waveform at $\mathcal{I}^+$ is described directly by $\tilde{\psi}_4$. Stage II provides indirect waveform information in terms of $\tilde{\psi}_0$, which can then be used to obtain the waveform by means of differential relations between $\tilde{\psi}_0$ and $\tilde{\psi}_4$. Asymptotically, at $\mathcal{I}^+$, these differential relations can be obtained either from the vacuum Bianchi identities [32] or from the asymptotic behavior of the metric [33–35]. Here we present the latter metric approach, since it provides a complete asymptotic description of Schwarzschild perturbations.

In the $(\tilde{u},r,x^A)$ Bondi coordinates with background Schwarzschild metric (2.3), a vacuum perturbation near $\mathcal{I}^+$ perturbs the metric in the asymptotically flat form [35]

$$\delta g_{ar}=\delta g_{AB}q^A\bar{q}^B=0, \tag{3.1}$$

$$\delta g_{\tilde{u}\tilde{u}}=\frac{2\mathcal{M}}{r}+O\left(\frac{1}{r^2}\right), \tag{3.2}$$

$$\delta g_{\tilde{u}A}q^A=\frac{\eth C}{4}+\frac{2\mathcal{L}}{3r}+O\left(\frac{1}{r^2}\right), \tag{3.3}$$

$$\delta g_{AB}q^Aq^B=Cr+\frac{Q}{r}+O\left(\frac{1}{r^2}\right), \tag{3.4}$$

where C, Q, $\mathcal{M}$ and $\mathcal{L}$ are spin-weighted functions of $(\tilde{u},x^A)$. The spin-weight-2 functions C and Q comprise the asymptotic part of the initial null data, in metric form, on a constant $\tilde{u}$ hypersurface. In Bondi's terminology, the spin-weight-0 function $\mathcal{M}$ is the (perturbed) mass aspect of the system and the spin-weight 1 function $\mathcal{L}$ is the angular momentum aspect. The time derivative of $\delta g_{AB}q^Aq^B$ can be determined from the evolution equations. The time derivative $\partial_{\tilde{u}}C$ is the Bondi news function and requires a radial integration to determine its value in terms of a boundary condition on an inner worldtube. The time derivative of Q can be determined locally. Similarly, the time derivatives of $\mathcal{M}$ and $\mathcal{L}$ can be determined locally from the components of Einstein's equations representing conservation laws. In an asymptotic Bondi frame, the relevant evolution-conservation equations are Eqs. (7.19)–(7.22) of Ref. [35]. They imply

$$\partial_{\tilde{u}}Q=\frac{\eth\mathcal{L}}{3}+\frac{\mathcal{M}C}{2}, \tag{3.5}$$

$$\partial_{\tilde{u}}\mathcal{M}=\frac{\eth^2\dot{\bar{C}}+\bar{\eth}^2\dot{C}}{16}, \tag{3.6}$$

$$\partial_{\tilde{u}}\mathcal{L}=\eth\mathcal{M}+\frac{\eth(\eth^2\bar{C}-\bar{\eth}^2C)}{16}. \tag{3.7}$$

The asymptotic values of the Weyl components are obtained from the metric according to

$$\tilde{\psi}_0^0:=\lim_{r\to\infty}r^5\tilde{\psi}_0=\frac{3}{2}Q, \tag{3.8}$$

$$\tilde{\psi}_4^0:=\lim_{r\to\infty}r\tilde{\psi}_4=\frac{1}{4}\partial_{\tilde{u}}^2\bar{C}. \tag{3.9}$$

This allows determination of $\tilde{\psi}_4^0$ in terms of $\tilde{\psi}_0^0$ by solving for C in terms of Q. By taking 2 $\tilde{u}$ derivatives of Eq. (3.5) and using Eqs. (3.6) and (3.7) to eliminate $\mathcal{M}$ and $\mathcal{L}$, we obtain

$$\partial_{\tilde{u}}^3Q=\frac{1}{24}\eth^4\partial_{\tilde{u}}\bar{C}+\frac{M}{2}\partial_{\tilde{u}}^2C. \tag{3.10}$$

Replacing C and Q by spin-weight 0 potentials defined by $C=\eth^2c$ and $Q=\eth^2q$, Eq. (3.10) reduces to

$$\partial_{\tilde{u}}^3q=\frac{1}{24}L^2(L^2-2)\partial_{\tilde{u}}\bar{c}+\frac{M}{2}\partial_{\tilde{u}}^2c. \tag{3.11}$$

When c is real, the solutions of Eq. (3.11) for which $q=0$ are solutions to the linearized Robinson-Trautman equation. Since the Robinson-Trautman solutions are singular as $\tilde{u}\to-\infty$, the requirement of nonsingular initial conditions leads to a one-to-one correspondence between c and q. The axisymmetric head-on collision of two black holes corresponds to the case where c is a real $(l=2,m=0)$ spherical harmonic. In that case, Eq. (3.11) gives

$$\partial_{\tilde{u}}c=\frac{2}{M}e^{-2\tilde{u}/M}\int_{-\infty}^{\tilde{u}}d\tilde{t}e^{2\tilde{t}/M}\partial_{\tilde{t}}^3q(\tilde{t}). \tag{3.12}$$

When c is complex, the solutions for $q=0$ correspond to a twisting version of a Robinson-Trautman perturbation. In this case, the imaginary part of c goes exponentially to ∞ as $\tilde{u}\to+\infty$ and the relation between c and q is more complicated. The complex case will not be considered further here.

For the quadrupole case, Eq. (3.11) determines the asymptotic relation at $\mathcal{I}^+$:

$$\frac{1}{6}\partial_{\tilde{u}}^4\tilde{F}_0=\tilde{F}_4+\frac{M}{2}\partial_{\tilde{u}}\tilde{F}_4, \tag{3.13}$$

which determines the waveform $\tilde{\psi}_4^0=\eth^2\tilde{F}_4^0$ at $\mathcal{I}^+$ in terms of the asymptotic field $\tilde{\psi}_0^0=\eth^2\tilde{F}_0^0$. This relation can also be expressed in the integral form

$$\tilde{\psi}_4^0=\partial_{\tilde{u}}\bar{N} \tag{3.14}$$

$$N=\frac{1}{4}\partial_{\tilde{u}}C=\frac{1}{2M}e^{-2\tilde{u}/M}\int_{-\infty}^{\tilde{u}}d\tilde{t}e^{2\tilde{t}/M}\partial_{\tilde{t}}^{3}Q(\tilde{t})$$

$$=\frac{1}{3M}e^{-2\tilde{u}/M}\int_{-\infty}^{\tilde{u}}d\tilde{t}e^{2\tilde{t}/M}\partial_{\tilde{t}}^{3}\tilde{\psi}_{0}^{0}(\tilde{t}), \tag{3.15}$$

where N is the Bondi news function.

IV. NUMERICAL ALGORITHMS AND ACCURACY

The stability of the background Schwarzschild geometry and the insensitivity of the Weyl tensor to gauge problems imply the absence of any theoretical limitations to the accurate numerical evolution of the Teukolsky equation in the exterior Kruskal quadrant, where the background spacetime is nonsingular. However, there is a practical limit to how close a numerical evolution can produce meaningful results near future time infinity I^+ or past time infinity I^-. There is no nonsingular way to treat time infinity as a boundary in a conformally compactified manifold, as is possible for null infinity. Thus time infinity can only be approached asymptotically and the asymptotic values of fields can depend on the direction of approach. This direction dependent limit at I^+ makes an evolution of ψ_0 difficult.

Numerical difficulties have led us to implement the stage II evolution of $\tilde{F}_0$ using two distinct approaches, one based upon a retarded time foliation and the other on an advanced time foliation. Both approaches require finding variables which allow for stable evolution of waves propagating inside the peak of the Schwarzschild potential, which turns out to be difficult. The retarded time algorithm uses an evolution variable which is adapted to the falloff at $\mathcal{I}^+$, and the advanced time algorithm uses an evolution variable adapted to the falloff at $\mathcal{I}^-$. Both approaches have similar accuracy but the advanced time algorithm is more efficient at treating behavior near $\mathcal{H}^+$ and the retarded time algorithm is more efficient near $\mathcal{I}^+$.

A. Retarded time algorithm

We base the retarded time algorithm on the evolution variable

$$\hat{F}_0=(1-2M/r)^2\tilde{F}_0, \tag{4.1}$$

which is finite on $\mathcal{H}^+$, as well as on $\mathcal{I}^+$ where the waveform is read off. However, the factor $(1-2M/r)^2$, which makes $\hat{F}_0$ vanish identically on $\mathcal{H}^-$, introduces a singularity at $\mathcal{H}^-$ in the associated Teukolsky equation. In addition, $\hat{F}_0$ is infinite on $\mathcal{I}^-$. We deal with these problems by initializing the double-null problem on an ingoing null hypersurface $\mathcal{K}^-$ approximating $\mathcal{H}^-$ and on an outgoing null hypersurface $\mathcal{J}^-$ approximating $\mathcal{I}^-$.

In $(\tilde{u},\tilde{v})$ double null coordinates, the Teukolsky equation for $\hat{F}_0$ $(l=2)$ is

$$\left(\partial_{\tilde{u}}\partial_{\tilde{v}}+\frac{2(1-2M/r)}{r}\partial_{\tilde{v}}-\frac{2M}{r^2}\partial_{\tilde{u}}+\frac{3M(1-2M/r)}{2r^3}\right)\hat{F}_0=0. \tag{4.2}$$

The code is implemented in coordinates $(\tilde{u},\rho)$, where $\rho=\arctan(\tilde{v}/\alpha)$ and α is an adjustable parameter (typically $\alpha=40M$). These coordinates compactify $\mathcal{I}^+$ at $\rho=\pi/2$. The Teukolsky equation takes the form

$$\partial_{\tilde{u}}\partial_{\rho}\hat{F}_0=-\frac{2(r-2M)}{r^2}\partial_{\rho}\hat{F}_0+\frac{2\alpha(1+\tan^2\rho)}{r^2}\partial_{\tilde{u}}\hat{F}_0$$
$$-\frac{3}{2}\frac{\alpha(r-2M)(1+\tan^2\rho)}{r^4}\hat{F}_0, \tag{4.3}$$

which is nonsingular in the region $-\pi/2<\rho<\pi/2$. However, compactification of $\mathcal{I}^+$ using double null coordinates necessarily leads to a loss of differentiability at $\mathcal{I}^+$ [36]. The coefficients in Eq. (4.3) have finite limits at $\mathcal{I}^+$, but the $\partial_{\tilde{u}}\hat{F}_0$ coefficient is not differentiable at $\mathcal{I}^+$. In $(\tilde{u},l=1/r)$ coordinates $\hat{F}_0$ can have analytic dependence on l at $\mathcal{I}^+$ but the transformation to $(\tilde{u},\rho)$ coordinates introduces logarithmic behavior so that $\hat{F}_0$ is not twice differentiable with respect to ρ at $\mathcal{I}^+$. Our tests show this still allows the computation of $\hat{F}_0$ on $\mathcal{I}^+$ to 2nd order accuracy in grid size. Similar logarithmic behavior exists at $\mathcal{I}^+$ in our original stage I algorithm [1].

We implement Eq. (4.3) as the first differential order system

$$\partial_{\tilde{u}}\hat{F}_0=g(\tilde{u},\rho)-\frac{2(r-2M)}{r^2}\hat{F}_0, \tag{4.4}$$

$$\partial_{\rho}g=\frac{2\alpha(1+\tan^2\rho)}{r^2}g-\frac{\alpha(1+\tan^2\rho)}{2r^4}$$
$$\times(r-2M)(3M+2r)\hat{F}_0, \tag{4.5}$$

where g is introduced as an auxiliary variable.

The numerical $(\tilde{u},\rho)$ grid consists of points on the $\tilde{u}=$const foliation. For reasons of economy and accuracy, the grid points are uniformly spaced in $\tilde{v}$ in the region of compact support where the initial data is non-zero and are uniformly spaced in ρ in the outer region where the initial data vanishes. We solve Eqs. (4.4) and (4.5) using a 2nd order accurate Runge-Kutta scheme.

B. Advanced time algorithm

We base the advanced time algorithm on the evolution variable

$$\check{F}_0=(1-2M/r)^2r\tilde{\Phi}_0=\frac{1}{r^4}\hat{F}_0, \tag{4.6}$$

which is finite on $\mathcal{I}^-$ and on $\mathcal{H}^+$. Since $\check{F}_0$ automatically vanishes on $\mathcal{H}^-$, we must again initialize on an ingoing null hypersurface $\mathcal{K}^-$ approximating $\mathcal{H}^-$. In addition, $\check{F}_0$ vanishes on $\mathcal{I}^+$. Consequently, the signal on $\mathcal{I}^+$ must be obtained by transforming $\check{F}_0$ to $\hat{F}_0$ on successively farther out $\tilde{v}=$const slices and extrapolating to $\tilde{v}=\infty$. Although the advanced time algorithm can be initialized on $\mathcal{I}^-$ this gives no distinct advantage in computing the waveform at $\mathcal{I}^+$ and, in order to facilitate comparison with the retarded time algorithm, we initialize on an outgoing null hypersurface $\mathcal{J}^-$ which approximates $\mathcal{I}^-$.

The advanced time evolution variable $\check{F}_0$ satisfies

$$\left(\partial_{\tilde{u}}\partial_{\tilde{v}}+\frac{2(r-3M)}{r^2}\partial_{\tilde{u}}+\frac{(1-2M/r)(2r+3M)}{2r^3}\right)\check{F}_0=0. \tag{4.7}$$

This is precisely the equation for $\tilde{F}_4$ under the transformation $\tilde{v}\leftrightarrow-\tilde{u}$. (Under time reflection, $\check{F}_0=4\mathcal{T}\tilde{F}_4$.) Thus the advanced time algorithm is equivalent to an algorithm for evolving $\tilde{F}_4$ backward in time.

The evolution proceeds along $\tilde{v}=$const null hypersurfaces, which are compactified by the coordinate transformation $\tilde{u}=\alpha\tan\mu$, where $-\pi/2\leqslant\mu\leqslant\pi/2$ in the range from $\mathcal{I}^-$ to $\mathcal{H}^+$, and α is again an adjustable parameter (typically $\alpha=200M$ in the advanced time case). In these coordinates, Eq. (4.7) becomes

$$\left(\partial_\mu\partial_{\tilde{v}}+\frac{2(r-3M)}{r^2}\partial_\mu+\frac{\alpha(1-2M/r)(2r+3M)}{2r^3\cos^2\mu}\right)\check{F}_0=0. \tag{4.8}$$

This equation is non-singular in the region $-\pi/2<\mu\leqslant\pi/2$, but the coefficient of $\check{F}_0$ is not differentiable on $\mathcal{I}^-$ ($\mu=-\pi/2$). On an ingoing null hypersurface, $\check{F}_0$ can be expressed as a power series in $l=1/r$. This implies that the associated series in μ contains logarithmic terms of the form $\mu(1+\mu\log\mu)$, and is not twice differentiable (with respect to μ) on $\mathcal{I}^-$. Our tests indicate that the code is 2nd order convergent despite this mild lack of differentiability.

We implement Eq. (4.8) in the first differential order form

$$\partial_\mu\check{F}_0=\check{g} \tag{4.9}$$

$$\partial_{\tilde{v}}\check{g}=-\frac{2(r-3M)\check{g}}{r^2}-\frac{\alpha(r-2M)(2r+3M)\check{F}_0}{2r^4\cos^2\mu}, \tag{4.10}$$

where we have introduced the auxiliary variable $\check{g}$. The numerical $(\mu,\tilde{v})$ grid consists of points on the $\tilde{v}=$const foliation equidistant in μ. The hypersurface equation (4.9) is solved by 2nd order accurate integration and Eq. (4.10) is solved by a 2nd order accurate Runge-Kutta scheme.

C. Extracting the retarded waveform

The retarded waveform $\tilde{F}_4$ on $\mathcal{I}^+$ is obtained from $\tilde{F}_0$ by means of Eq. (3.13). Given the values of $\tilde{F}_0$, we integrate Eq. (3.13) by the midpoint rule to obtain $\tilde{F}_4$, using the initial condition that $\tilde{F}_4=0$.

The retarded algorithm provides $\tilde{F}_0$ on $\mathcal{I}^+$ directly. In the advanced algorithm, where $\mathcal{I}^+$ is not in the evolution domain, we extrapolate the waveform at $\mathcal{I}^+$ from a quadratic polynomial based upon approximate values of $\tilde{F}_4$ obtained by applying Eq. (3.13) on three ingoing null hypersurfaces approximating $\mathcal{I}^+$ (where we substitute $r^4\check{F}_0$ for $\tilde{F}_0$). The three null hypersurfaces consist of the advanced time slices $\tilde{v}_f$, $\tilde{v}_f/2$, and $\tilde{v}_f/3$, where (typically) $\tilde{v}_f=4000M$.

D. Initializing the stage II evolution

Initial data for the stage II evolution, i.e. the value of $\tilde{\psi}_0$ on $\mathcal{J}^-$, is obtained by a time reflection of the retarded stage I solution for $\tilde{\psi}_4$ on $\mathcal{J}^+$. Technical problems arise here because the stage I evolution does not provide accurate data at late times on $\mathcal{J}^+$ [1]. We deal with this by smoothing the stage II initial data to zero outside a region of compact support where the data would otherwise be small. This modification of the initial data also guarantees consistency with the boundary data $\psi_0=0$ on $\mathcal{K}^-$, which approximates the boundary condition that the perturbation vanishes on $\mathcal{H}^-$.

The relation $\tilde{\psi}_4^0=\partial_{\tilde{u}}\overline{N}$ on $\mathcal{I}^+$ requires that the integral

$$\int_{-\infty}^{\infty}d\tilde{u}\,\tilde{\psi}_4^0=\overline{N}\big|_{-\infty}^{\infty} \tag{4.11}$$

vanish since the news function N must vanish at either limit in order that the radiated mass loss be finite. By time reflection, it follows that the integral

$$\int_{-\infty}^{\infty}d\tilde{v}\check{F}_0=0 \tag{4.12}$$

on $\mathcal{I}^-$. However, artificially truncating the initial data to compact support causes this integral to be non-zero, although small. This leads to the following artificial behavior of $\tilde{F}_0$ at early retarded times.

This early time behavior of $\check{F}_0$ is conveniently described in coordinates $(\tilde{v},l=1/r)$ which compactify $\mathcal{I}^-$ at $l=0$. In these coordinates, the evolution Eq. (4.8) becomes

$$\left[\partial_l\partial_{\tilde{v}}+\left(l^3M-\frac{1}{2}l^2\right)\partial_l^2+(l-3l^2M)\partial_l+(2+3Ml)\right]\check{F}_0=0. \tag{4.13}$$

Consider initial data on $\mathcal{I}^-$ with compact support in the region $\tilde{v}_a<\tilde{v}<\tilde{v}_b$. Integration of Eq. (4.13) along $\mathcal{I}^-$ from $\tilde{v}=\tilde{v}_a$ to $\tilde{v}$ yields

$$\partial_l\check{F}_0=-2\int_{\tilde{v}_a}^{\tilde{v}}d\tilde{v}\check{F}_0d\tilde{v}=a(\tilde{v}),$$

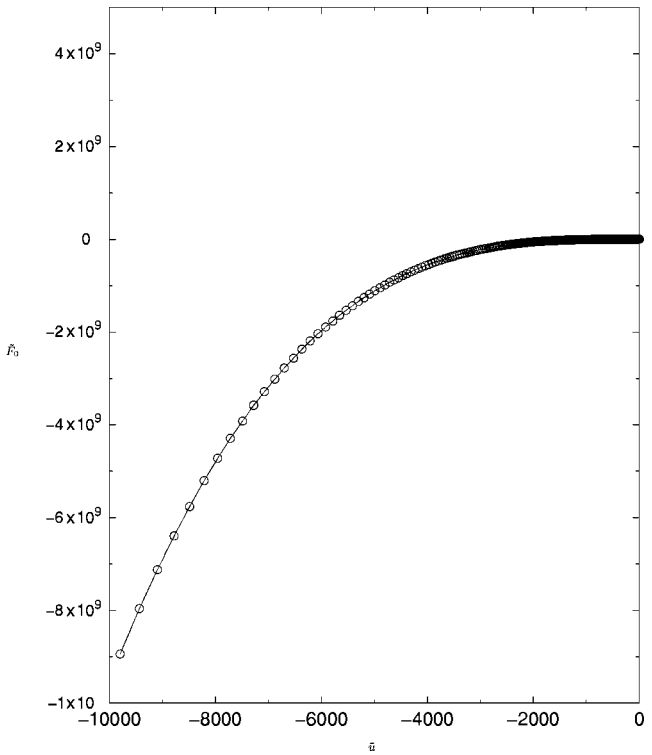

FIG. 1. Signal $\tilde{F}_0(\tilde{u})$ produced on $\tilde{v}=1000M$ by an initial compact pulse. The solid curve indicates a fit to a cubic polynomial.

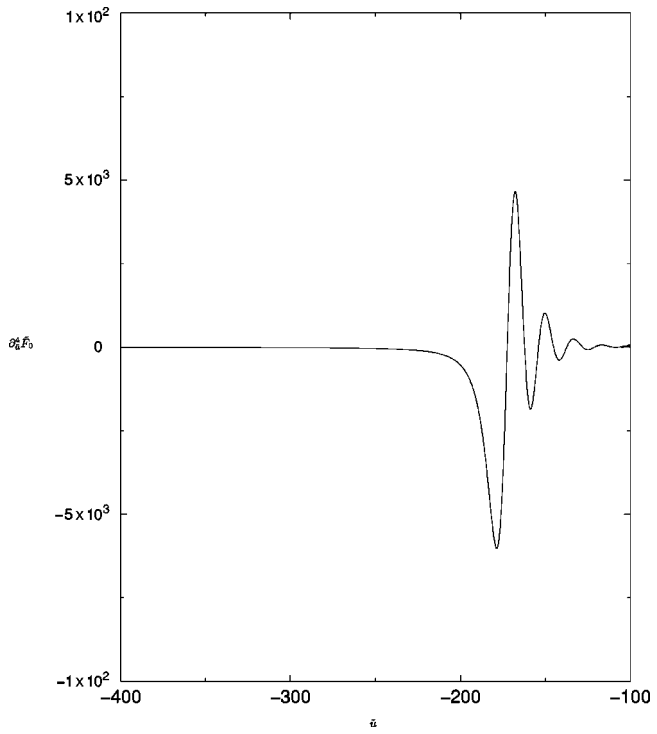

FIG. 2. The 4th $\tilde{u}$-derivative of Fig. 1.

where according to the above argument $a(\tilde{v})$ should vanish for $\tilde{v}\geqslant\tilde{v}_b$. However, our numerical procedure for truncating the data leads to a small value of $a(\tilde{v}_b)$. Hence, for $\tilde{v}\geqslant\tilde{v}_b$, on any ingoing null hypersurface, $\check{F}_0$ has the asymptotic behavior $\check{F}_0(\tilde{v},l)=a(\tilde{v}_b)l+O(l^2)$. When re-expressed in $(\tilde{u},\tilde{v})$ double null coordinates, this implies $\tilde{F}_0$ has the asymptotic behavior $\tilde{F}_0(\tilde{u},\tilde{v})=a(\tilde{v}_b)\tilde{u}^3+O(\tilde{u}^2)$. In numerical simulations, this produces artificial cubic polynomial dependence of $\tilde{F}_0$ at early times on $\mathcal{I}^+$. Since this cubic behavior is removed by taking four $\tilde{u}$-derivatives it does not affect the waveform $\tilde{F}_4$ calculated from $\tilde{F}_0$ using Eq. (3.13).

We simulated this artificial early time behavior by using the advanced time algorithm to propagate an extremely narrow initial compact support pulse on $\mathcal{I}^-$ of the form $\check{F}_0=[(\tilde{v}-\tilde{v}_1)(\tilde{v}_2-\tilde{v})]^4$ for $\tilde{v}_1<\tilde{v}<\tilde{v}_2$, and $\check{F}_0=0$ otherwise, where $\tilde{v}_2-\tilde{v}_1=.1M$. Figure 1 plots the resulting signal $\tilde{F}_0$ on the ingoing null hypersurface $\tilde{v}=1000M$. (By looking at the signal on finite $\tilde{v}$ we avoid problems associated with spatial infinity i^0.) The figure shows that the early time behavior fits a cubic polynomial in $\tilde{u}$. This cubic polynomial dominates at later times and masks physical effects such as quasinormal ringdown. However, Fig. 2 shows that after taking four $\tilde{u}$-derivatives the ringdown is clearly observed and there is little trace of the secular behavior. Note the drastic difference between the scales of Figs. 1 and 2.

In computing waveforms from close approximation data, because the initial surface $\mathcal{J}^-$ is at finite $\tilde{u}$ the artificial early time behavior in $\tilde{F}_0$ is described by a quartic rather than cubic polynomial in $\tilde{u}$ but the 4th order coefficient is small for reasonably early start times. We performed the following experiments to measure the sensitivity of the stage II signal to the location of $\mathcal{K}^-$ and $\mathcal{J}^-$. In these experiments we used a stage I run to obtain close approximation initial data with $\eta=1410$ for $\tilde{F}_0$ on $\mathcal{J}^-$ and measured the signal propagated to $\mathcal{I}^+$. Except when computational expense would have been prohibitive, the experiments were carried out with both the retarded time and advanced time evolution algorithms with virtually equivalent results.

In the first set of experiments, $\mathcal{K}^-$ was placed at $\tilde{v}=-200M$ and $\tilde{v}=-100M$, with the initial hypersurface $\mathcal{J}^-$ located at $\tilde{u}=-720M$ in both cases. For $\tilde{v}=-100M$ the initial data on $\mathcal{J}^-$ implied by the time reflection of the stage I evolution was approximately 5 orders of magnitude smaller at $\mathcal{K}^-$ than at its peak (at $\tilde{v}\approx 0$); and for $\tilde{v}=-200M$, the size at $\mathcal{K}^-$ was 9 orders of magnitude smaller than at the peak. The stage II approximation of smoothing these data to zero on $\mathcal{K}^-$ violates the integral condition (4.12) and produces the early time polynomial behavior shown in the plots of $\tilde{F}_0(\tilde{u})$ at $\mathcal{I}^+$ in Fig. 3. For both locations of $\mathcal{K}^-$ the early time behavior is well fit by a 4th order polynomial but the size of the polynomial is about 10^7 times larger for the farther out location of $\mathcal{K}^-$.

Figure 4 is a magnified view of Fig. 3 showing how the early time quartic polynomial behavior contaminates the genuine signal at later times.

Figure 5 shows that the two signals agree after taking four $\tilde{u}$ derivatives.

In the second set of experiments, $\mathcal{J}^-$ was located at $\tilde{u}$

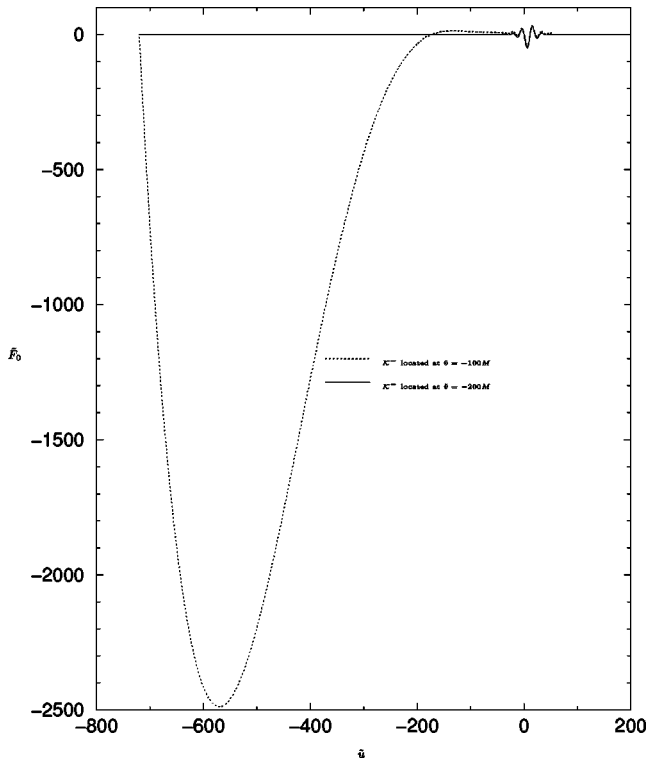

FIG. 3. Comparison of the behavior of $\tilde{F}_0$ for two locations of $\mathcal{K}^-$.

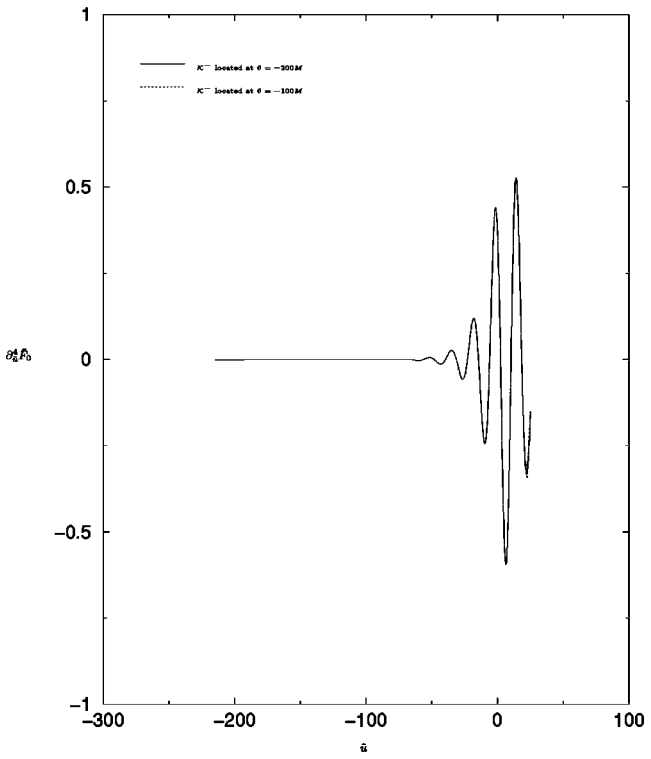

FIG. 5. The 4th $\tilde{u}$ derivative of Fig. 3 shows independence of the location of $\mathcal{K}^-$. The evolution is terminated when late time noise begins to contaminate the results. (See Sec. IV E.)

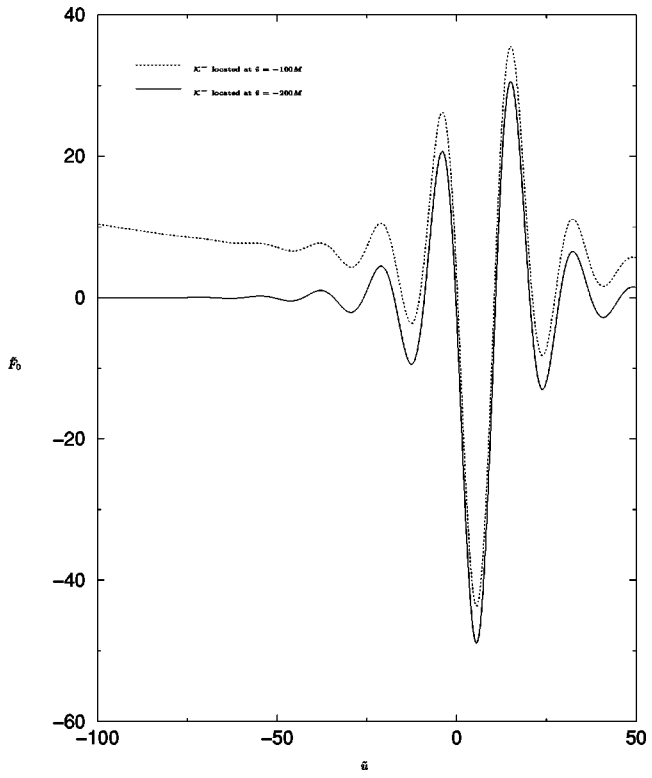

FIG. 4. Blowup of Fig. 3 in the region of the genuine signal.

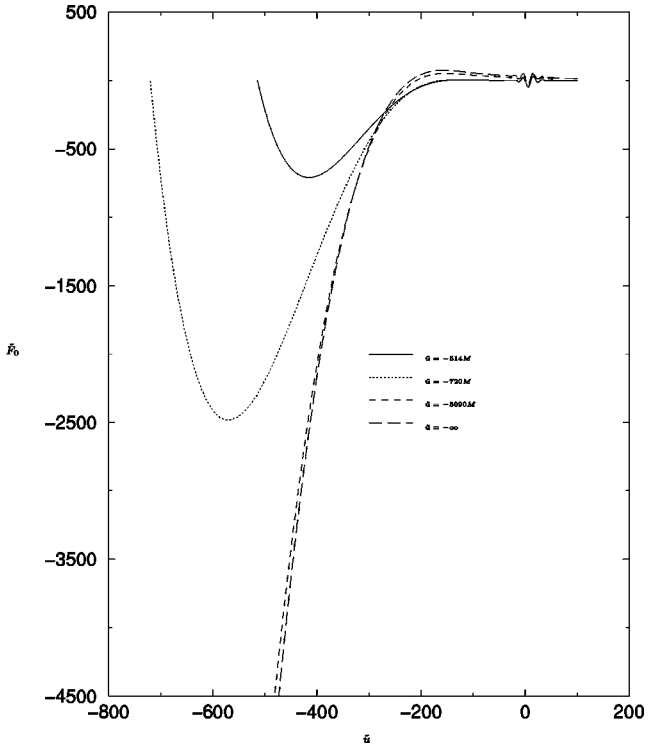

FIG. 6. Comparison of early time behavior for $\mathcal{J}^-$ located at four different retarded times.

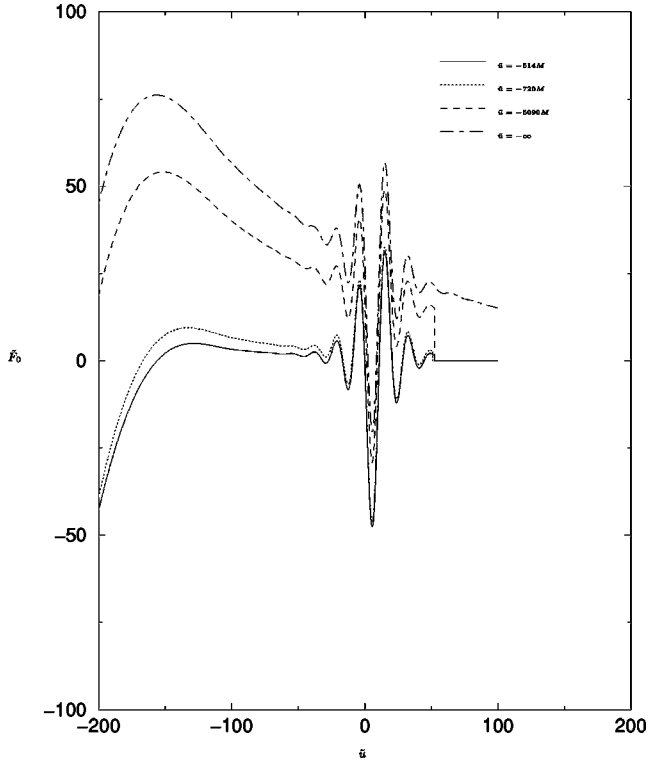

FIG. 7. Blowup of Fig. 6.

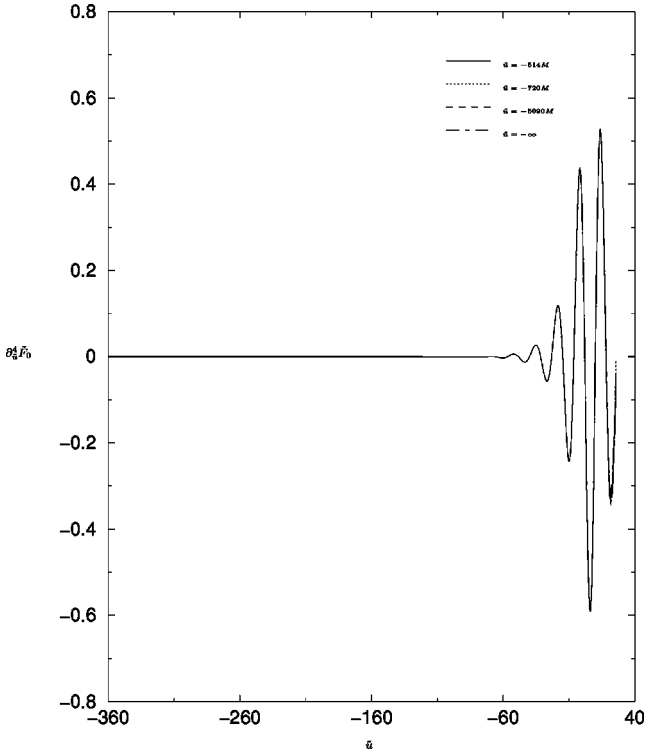

FIG. 8. The 4th $\tilde{u}$ derivative of Fig. 7 showing the independence on the location of $\mathcal{J}^-$.

$=-540M$, $\tilde{u}=-720M$, $\tilde{u}=-5090M$, and $\tilde{u}=-\infty$, with $\mathcal{K}^-$ located at $\tilde{v}=-100M$ (to accentuate the early time polynomial behavior). Figure 6, which plots the resulting signal $\tilde{F}_0(\tilde{u})$ on $\tilde{v}=1000M$, shows that the polynomial behavior becomes more pronounced as $\mathcal{J}^-$ approaches $\mathcal{I}^-$.

Figure 7 shows how the early time polynomial contaminates the genuine signal at later times, with the effect increasing as $\mathcal{J}^-$ is located farther in the past. Finally, Fig. 8 shows that $\partial_{\tilde{u}}^4 \tilde{F}_0$ is unaffected by the artificial polynomial behavior and indicates that a start time of $\tilde{u}=-500M$ is sufficiently early to obtain the correct stage II retarded waveform on $\mathcal{I}^+$.

Both sets of experiments confirm that the artificial behavior of $\tilde{F}_0$ at early times has no effect on the accurate calculation of the waveform at $\mathcal{I}^+$.

E. Late time behavior

Both the retarded time and advanced time algorithms exhibit exponentially increasing errors at late times. This numerical problem arises from the definition of our evolution variables, which are not designed to deal with late time features near the future horizon $\mathcal{H}^+$. For $r\approx 2M$, our evolution variables are related to the Israel tetrad variable F_0 by

$$\hat{F}_0 = 16M^4 \check{F}_0 = \frac{\lambda^2}{4M^2} F_0, \tag{4.14}$$

where the affine parameter λ is exponentially related to advanced Bondi time by

$$\lambda = 8M e^{(\tilde{v}/4M)-1}.$$

Because F_0 is defined in terms of a globally well-behaved tetrad, this introduces an exponential dependence in the evolution variables which influences the numerical performance in the following way.

Near $\mathcal{H}^+$, as $r\to 2M$, Eqs. (4.2) and (4.7) reduce to

$$\left(\partial_{\tilde{v}} - \frac{1}{2M}\right)\partial_{\tilde{u}} f_0 = 0, \tag{4.15}$$

where $f_0 = \hat{F}_0 = 16M^4 \check{F}_0$. This equation admits outgoing waves of the form $f_0 = f(\tilde{u})\exp(\tilde{v}/(2M))$ in the region inside the Schwarzschild potential. These exponentially growing waves are forbidden in the analytic version of our problem by the boundary condition that $\hat{F}_0 = \check{F}_0 = 0$ on $\mathcal{K}^-$ but they are excited by roundoff error. As the computation proceeds, the interval $\Delta\tilde{v}$ between $\mathcal{K}^-$ and the peak of the Schwarzschild potential increases and eventually round-off error in this interval undergoes sufficient exponential magnification to spoil the exterior evolution. There remains an inner region on $\mathcal{H}^+$ where the solution is accurate. For both algorithms, doubling the precision at which the computation is carried out increases the meaningful computation time. For example, the double precision runs shown in Figs. 5 and 8 end prematurely due to the onset of numerical noise but in quadruple precision both runs can be extended through five or six cycles of quasinormal ringdown.

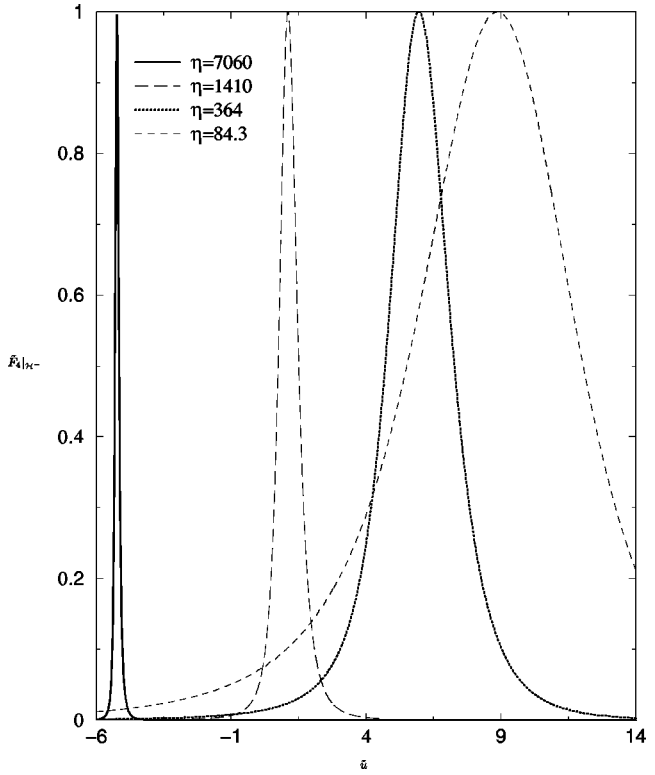

FIG. 9. White hole fission close approximation data $\tilde{F}_4(\tilde{u})$ on $\mathcal{H}^-$ for $\eta=7060$, 1410, 364 and 84.3.

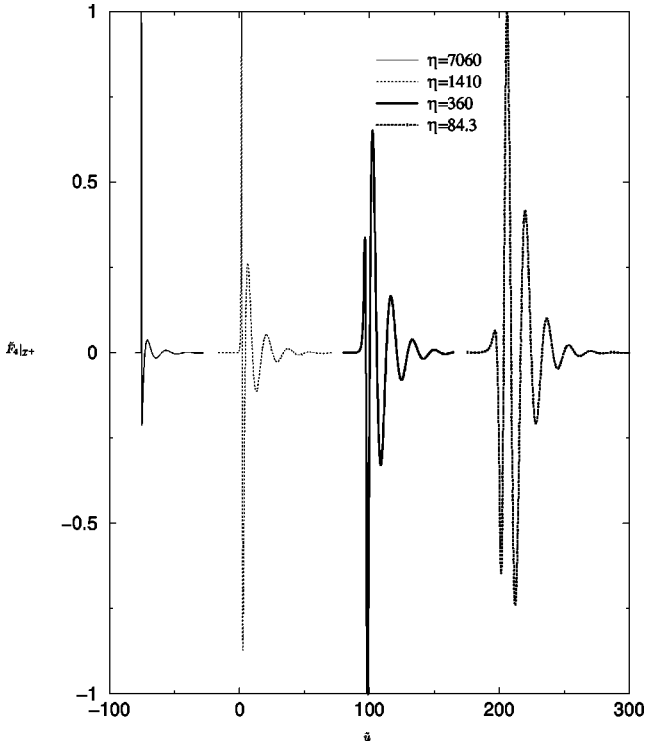

FIG. 10. Close approximation waveforms $\tilde{F}_4(\tilde{u})$ on $\mathcal{I}^+$ for $\eta=7060$, 1400, 368 and 84.3.

V. CLOSE APPROXIMATION RETARDED WAVEFORMS

We begin with a review of the close approximation retarded waveforms from a white hole fission obtained in stage I [1]. The close approximation white hole horizon perturbation ($\tilde{F}_4|_{\mathcal{H}^-}$) given by the conformal model is a pulse with the following basic properties in terms of its dependence on the scale invariant parameter η (see Sec. II A). In the large η limit ($\eta>250$) the amplitude of the pulse scales quadratically with η and the width is a monotonically decreasing function of η (the width becomes zero as $\eta\to\infty$). In the small η limit ($\eta<25$) the amplitude scales linearly with η but the shape of the pulse is independent of η. Figure 9 shows the horizon data obtained from various large and mid-size values of η (the amplitudes have been renormalized so that all pulses have the same height).

The associated retarded white hole fission waveforms ($\tilde{F}_4|_{\mathcal{I}^+}$) have a similar dependence on η. In the large η limit the waveform consists of an extremely sharp initial pulse followed by ringdown and power law tail. The amplitude of the initial pulse scales quadratically with η and the width is a monotonically decreasing function of η. As η is reduced, the initial pulse (signal prior to ringdown) becomes wider and obtains more structure. In the small η limit the amplitude scales linearly with η and the shape is independent of η. Figure 10 shows a sequence of waveforms from large to mid-size values of η.

We now present the results for the retarded solutions from a black hole fusion in the close approximation obtained by

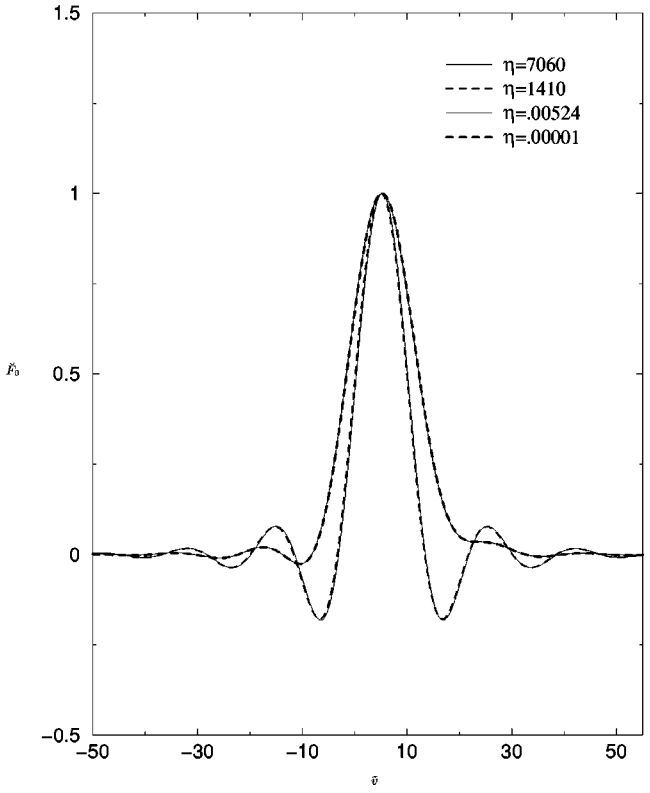

FIG. 11. Final black hole horizon perturbation after superposing stage I and II, with amplitudes renormalized so that the peaks match. The narrow peak corresponds to $\eta=7060$ and $\eta=1410$.

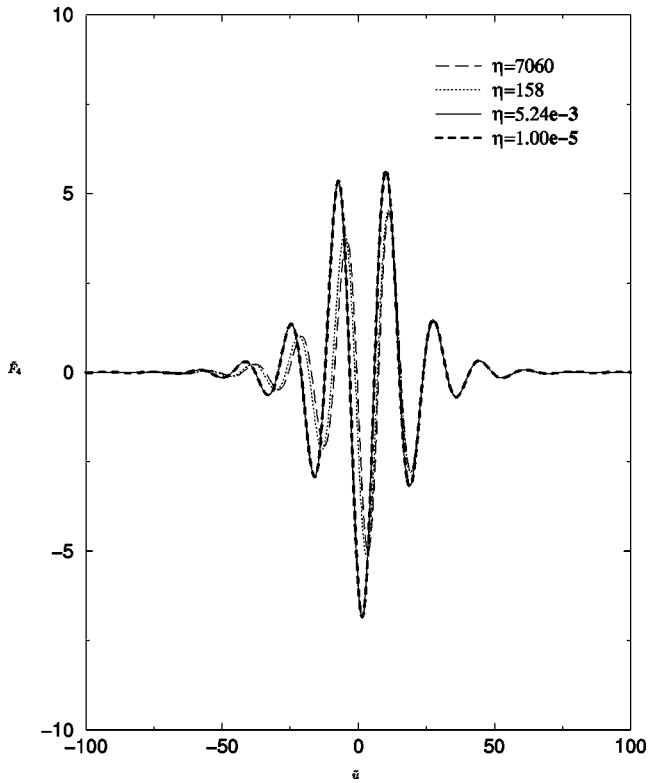

FIG. 12. Black hole retarded waveforms for close approximation data.

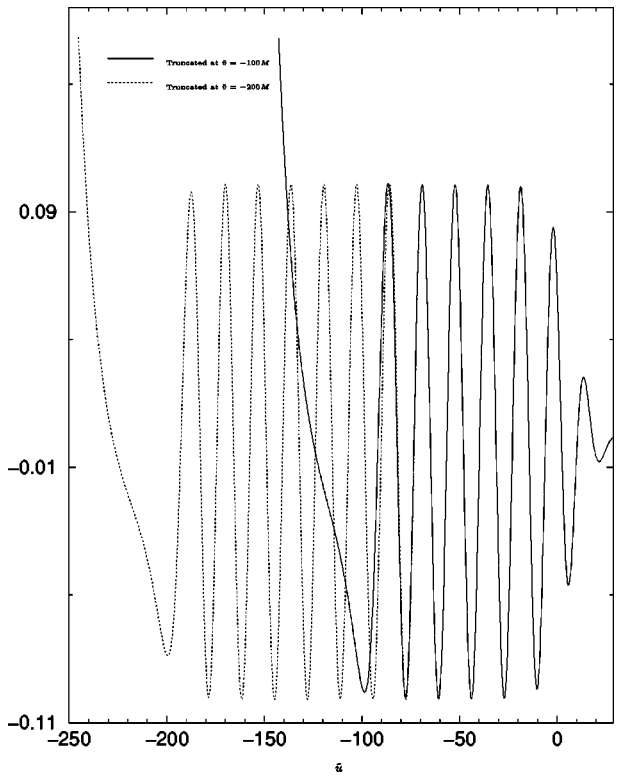

FIG. 13. Ringup of the waveform: $\tilde{F}_4|_{\mathcal{I}^+}$ multiplied by $\exp -.08896\tilde{u}/M$.

superposition of the advanced black hole results (time reversal of the above white hole solutions) and the stage II results. This superposition yields the retarded waveform and a modified black hole horizon perturbation. In the following paragraph, we first describe the black hole horizon perturbations.

Figure 11 shows the perturbation on $\mathcal{H}^+$ for the retarded black hole solution. Unlike the stage I perturbation of the white hole horizon (see Fig. 9), here the width of the perturbation is never smaller than a quasinormal period.

The superposition procedure for obtaining the stage II perturbation of the black hole horizon turns the very sharp stage I pulses associated with large η into relatively broad pulses. The final black hole perturbation approaches a unique asymptotic shape in both the large and small η limits. In Fig. 11, $\eta=7060$ and $\eta=1410$ give the large η shape, while $\eta=.00524$ and $\eta=.00001$ give the same small η shape. Note that the two extremes are themselves very similar. Consequently all the retarded black hole waveforms obtained from this procedure are very similar in shape.

One of the most striking features of this new horizon perturbation is the initial ringup, which is later followed by the expected ringdown due to scattering off the Schwarzschild potential. The ringup on $\mathcal{H}^+$ results from the ringup of the data on $\mathcal{J}^-$, which in turn results from the ringdown of the stage I waveform. This ringup is an unavoidable feature of our two stage methodology for removing ingoing radiation from the black hole merger.

Figure 12 shows the waveforms for close approximation data obtained from the conformal model. The amplitude of the waveforms scales linearly with η and has been renormalized so that all waveforms show the same quasinormal decay at late times. Note that, aside from amplitude, the waveforms have only weak dependence on η. This is a great departure from the stage I results that the widths of the retarded white hole waveforms depend strongly on η, which produces extremely narrow pulses for large η.

It should not be surprising that retarded waveforms from a black hole merger differ qualitatively from retarded waveforms from a white hole fission. The fission process is directly observable at $\mathcal{I}^+$, whereas the merger waveform results indirectly from the black holes through the preceding collapse of matter or gravitational wave energy that formed them. This also explains why the fission waveform should be more sensitive to the parameter η which controls the shape and time scale of the horizon data. However, the weakness of the dependence of the merger waveform on η is surprising.

The retarded black hole waveforms at $\mathcal{I}^+$ also show the ringup-ringdown pattern. The ringup is due to backscatter of the ringup on the initial slice $\mathcal{J}^-$. Interestingly, the backscattered signal of an $l=2$ quasinormal ringup on $\mathcal{J}^-$ is a ringup on $\mathcal{I}^+$ with the same $l=2$ time dependence. Figure 13 shows the ringup phase of the waveform obtained by placing $\mathcal{K}^-$ at $\tilde{v}=-100M$ and at $\tilde{v}=-200M$. (The data for $\tilde{v}=-200M$ contain more ringup cycles.) In the figure $\tilde{F}_4|_{\mathcal{I}^+}$ is multiplied by $\exp(0.08896\tilde{u})$ to remove the exponential part of the quasinormal time dependence. Note that in the $\tilde{v}=-200M$ case the ringup begins exactly $100M$ sooner indicating that it is indeed the ringup of the initial data that is responsible for the ringup of the waveform on $\mathcal{I}^+$.

VI. DISCUSSION

We have combined the conformal horizon model with a null evolution code to give a new way to calculate the retarded waveform from a binary black hole merger in the close approximation. The process of removing ingoing radiation from the system leads to two major new features in the shape of the close approximation waveforms for a head-on collision: (i) an initial quasinormal ringup and (ii) weak sensitivity to the parameter η of the model that in some heuristic sense controls the collision velocity. Feature (ii) has the potential importance of enabling the design of an efficient template for extracting a gravitational wave signal from noise.

Similar attempts to remove ingoing radiation from Cauchy evolutions of close approximation data have not yet been made. Such studies would help clarify whether the above features are of intrinsic physical origin or an artifact of our methodology.

The present work is part of an ongoing effort to carry out a similar two stage characteristic evolution to provide the waveforms from coalescing black holes in the nonlinear regime. Because this is an unexplored area of binary black hole physics, this perturbative study of the head-on collision provides a preliminary physical check which will be useful in extending the work to the nonlinear and nonaxisymmetric case, where inspiraling black holes can be treated.

ACKNOWLEDGMENTS

We thank Manuela Campanelli for numerous helpful discussions. This work has been supported by NSF grants PHY 9800731 and PHY 9988663 to the University of Pittsburgh and PHY-0135390 to Carnegie Mellon University. Y.Z. thanks the Albert-Einstein-Institut for hospitality. Computer time for this project has been provided by the Pittsburgh Supercomputing Center.

[1] M. Campanelli, R. Gómez, S. Husa, J. Winicour, and Y. Zlochower, Phys. Rev. D **63**, 124013 (2001).
[2] S. Brandt, R. Correll, R. Gomez, M. Huq, P. Laguna, L. Lehner, P. Marronetti, R.A. Matzner, D. Neilsen, J. Pullin, E. Schnetter, D. Shoemaker, and J. Winicour, Phys. Rev. Lett. **85**, 5496 (2000).
[3] M. Alcubierre, W. Benger, B. Bruegmann, G. Lanfermann, L. Nerger, E. Seidel, and R. Takahashi, Phys. Rev. Lett. **87**, 271103 (2001).
[4] R.H. Price and J. Pullin, Phys. Rev. Lett. **72**, 3297 (1994).
[5] Z. Andrade and R. Price, Phys. Rev. D **56**, 6336 (1997).
[6] M. Campanelli, W. Krivan, and C.O. Lousto, Phys. Rev. D **58**, 024016 (1998).
[7] M. Campanelli and C.O. Lousto, Phys. Rev. D **58**, 024015 (1998).
[8] M. Campanelli, C.O. Lousto, J. Baker, G. Khanna, and J. Pullin, Phys. Rev. D **58**, 084019 (1998).
[9] C.O. Nicasio, R. Gleiser, R. Price, and J. Pullin, Phys. Rev. D **59**, 044024 (1999).
[10] W. Krivan and R. Price, Phys. Rev. Lett. **82**, 1358 (1999).
[11] G. Khanna, J. Baker, R. Gleiser, P. Laguna, O. Nicasio, H.-P. Nollert, R. Price, and J. Pullin, Phys. Rev. Lett. **83**, 3581 (1999).
[12] M. Campanelli and C.O. Lousto, Phys. Rev. D **59**, 124022 (1999).
[13] J. Baker, B. Brügmann, M. Campanelli, and C.O. Lousto, Class. Quantum Grav. **17**, L149 (2000).
[14] O. Sarbach, M. Tiglio, and J. Pullin, Phys. Rev. D **65**, 064026 (2002).
[15] J. Baker, S. Brandt, M. Campanelli, C.O. Lousto, E. Seidel, and R. Takahashi, Phys. Rev. D **62**, 127701 (2000).
[16] E. Seidel, in *On the Black Hole Trail*, edited by B.R. Iyer and B. Bhawal (Kluwer, Dordrecht, 1998).
[17] G. Allen, K. Camarda, and E. Seidel, ''Evolution of Distorted Black Holes: A Perturbative Approach,'' gr-qc/9806014.
[18] N.T. Bishop, R. Gómez, L. Lehner, M. Maharaj, and J. Winicour, Phys. Rev. D **56**, 6298 (1997).
[19] J. Winicour, Prog. Theor. Phys. Suppl. **136**, 57 (1999).
[20] R. Gómez, S. Husa, and J. Winicour, Phys. Rev. D **64**, 024010 (2001).
[21] R. Gómez, S. Husa, L. Lehner, and J. Winicour, ''Gravitational Waves from a Fissioning White Hole'' (in preparation).
[22] R. Gómez, Phys. Rev. D **64**, 024007 (2001).
[23] R. Sachs, J. Math. Phys. **3**, 908 (1962).
[24] S.A. Hayward, Class. Quantum Grav. **10**, 779 (1993).
[25] H. Friedrich, Proc. R. Soc. London **A378**, 401 (1981).
[26] A.H. Rendall, Proc. R. Soc. London **A427**, 221 (1990).
[27] S.A. Teukolsky, Astrophys. J. **185**, 635 (1973).
[28] W. Israel, Phys. Rev. **143**, 1016 (1966).
[29] E.T. Newman and R. Penrose, J. Math. Phys. **3**, 566 (1962).
[30] L. Lehner, N.T. Bishop, R. Gómez, B. Szilágyi, and J. Winicour, Phys. Rev. D **60**, 044005 (1999).
[31] S. Husa and J. Winicour, Phys. Rev. D **60**, 084019 (1999).
[32] E.T. Newman and T.W.J. Unti, J. Math. Phys. **5**, 891 (1962).
[33] H. Bondi, M.J.G. van der Burg, and A.W.K. Metzner, Proc. R. Soc. London **A269**, 21 (1962).
[34] R.K. Sachs, Proc. R. Soc. London **A270**, 103 (1962).
[35] L. Tamburino and J. Winicour, Phys. Rev. **150**, 1039 (1966).
[36] B.G. Schmidt, in *The Conformal Structure of Spacetime: Gravity, Analysis, Numerics*, edited by J. Frauendiener and H. Friedrich (Springer, Berlin, in press).